# Toward functional ultrasound-modulated optical tomography: a phantom study

Chulhong Kim, Lihong V. Wang

Chulhong Kim, Lihong V. Wang, "Toward functional ultrasound-modulated optical tomography: a phantom study," Proc. SPIE 6856, Photons Plus Ultrasound: Imaging and Sensing 2008: The Ninth Conference on Biomedical Thermoacoustics, Optoacoustics, and Acousto-optics, 68561U (28 February 2008); doi: 10.1117/12.761377

SPIE.

Event: SPIE BiOS, 2008, San Jose, California, United States

# Toward functional ultrasound-modulated optical tomography: a phantom study

Chulhong Kim and Lihong V. Wang*

Optical Imaging Laboratory, Department of Biomedical Engineering, Washington University in St. Louis, Campus Box 1097, One Brookings Dr. St. Louis, Missouri, 63130

## ABSTRACT

We present the feasibility of functional ultrasound-modulated optical tomography (UOT) in tissue phantoms with two optical wavelengths. By using intense acoustic bursts and a CCD camera-based speckle contrast detection technique, we observe variations of UOT signal at different optical absorptions. In addition, the results from Monte Carlo simulations highly correlate with the experimental outcomes. By irradiating the sample at two optical wavelengths, we quantitatively estimate the total concentration and the concentration ratio of double dyes in inclusions inside tissue phantoms. Therefore, UOT is potentially able to supply functional imaging of the total concentration and oxygen saturation of hemoglobin non-invasively in biological tissues.

**Keywords:** Ultrasound-modulated optical tomography, total hemoglobin concentration, oxygen saturation of hemoglobin, functional imaging.

## INTRODUCTION

### 1. Motivation

Imaging functional information of living subjects, such as the total hemoglobin concentration (HbT) and hemoglobin oxygen saturation ($SO_2$), has become important in many medical fields, for examples, imaging normal and abnormal brain activation[1] and studying tumor physiopathology[2]. Currently, a few non-ionizing-optical imaging techniques, such as diffuse optical tomography (DOT)[3] and photoacoustic imaging[4,5], can estimate the HbT and $SO_2$ in living subjects non-invasively. Due to strong light scattering in biological tissue, however, pure optical imaging techniques like DOT suffer from poor spatial resolution which degrades with increasing imaging depth. Photoacoutic imaging overcomes such drawbacks of DOT because its spatial resolution depends on ultrasound parameters, whose scattering is 2–3 orders of magnitude weaker than light scattering in biological tissues. Similar to photoacoustic imaging, ultrasound-modulated optical tomography (UOT)[6] is able to provide strong optical contrast and high ultrasonic spatial resolution. Therefore, thanks to the strong optical contrast, UOT has potential for functional imaging.

The principles of UOT is that multiply scattered light passing through an ultrasonic focal volume is acoustically phase-modulated by both ultrasound-induced particle displacement and changes in refractive index. By computing the ratio of the ultrasound-modulated light intensity to the unmodulated light intensity at each scanned ultrasonic focal volume, images represent the optical heterogeneities of the tissue. The mechanisms of UOT has been theoretically studied by Leutz et al.[7], Wang[8], and Sakadžic´ and Wang[9,10]. Because of the low modulation efficiency and uncorrelated speckle grains, low signal-to-noise ratio (SNR) is a major problem in UOT. A number of detection techniques have been pioneered to detect weak modulated signals efficiently such as parallel speckle detection using a CCD camera[11], photorefractive crystal based detection[12], fabry-perot interferometer based detection[13]. Rather than devoting efforts to the detection of weak signals, Kim et al. and Zemp et al.[14,15] explored the use of intense acoustic bursts as a significant signal enhancement mechanism. Recently, Xu *et al*.[16] and Bossy *et al*.[17] reported the measurement of mechanical contrast of tissues using UOT in detail. In this Proceedings artile, we applied two optical wavelengths to UOT toward studying the feasibility of functional imaging, total hemoglobin concentration and hemoglobin saturation of oxygen, of tissue. By using intense acoustic bursts and using the speckle contrast detection technique[14,15] at two optical

* Corresponding author: lhwang@biomed.wustl.edu

Photons Plus Ultrasound: Imaging and Sensing 2008: The Ninth Conference on Biomedical Thermoacoustics, Optoacoustics, and Acousto-optics, edited by Alexander A. Oraevsky, Lihong V. Wang, Proc. of SPIE Vol. 6856, 68561U, (2008) · 1605-7422/08/$18 · doi: 10.1117/12.761377

wavelengths, we quantitatively estimated the relative total concentration of red and blue dye mixtures and the ratio of the red dye concentration to the total concentration in inclusions in tissue mimicking phantoms. In addition, the variation of UOT signals at various optical absorptions was modeled with Monte Carlo simulations and compared with the experimental results.

## EXPERIMENT

The experimental schematic is shown in Fig. 1. Two lasers (JDS Uniphase, HeNe 1145; 633-nm wavelength and Melles Griot, 56ICS153/HS; 657-nm wavelength) illuminated a tissue mimicking phantom sequentially. An average laser power of ~30 mW/cm$^2$ was delivered to the tissue phantom. A 1-MHz focused ultrasound transducer with 25 mm active aperture and 38 mm focal length (Ultran, VHP100-1-138) generated acoustic waves. The ultrasonic focal zone was ~2 mm in diameter and ~20 mm in length. An ultrasound peak pressure of less than 1.9 MPa was applied to the focal point. Therefore, the mechanical index at this frequency was smaller than 1.9, which is within the typical safety limit for diagnostic ultrasound.[18] We used a gelatin-cornstarch phantom (10% gelatin and 10% cornstarch by weight) whose optical reduced scattering coefficient was ~9 cm$^{-1}$ at both wavelengths measured by the oblique-incidence diffuse reflectance spectroscopy.[19] A red dye was made from the mixture of Fiesta Red and India Red inks, whereas a blue dye was made of Trypan Blue. The absorption coefficients of the red dye in the mother liquid at 633- and 657-nm wavelengths measured by the light transmission were ~2.2 and ~1.0 cm$^{-1}$, respectively, whereas the ones of the blue dye in the mother liquid at the two wavelengths were ~11.9 and ~5.2 cm$^{-1}$, respectively. The optically absorptive targets were made of the dye solutions and 10% gelatin. A CCD camera (Basler, A312f; 12-bit, 640×480 pixels) captured speckle patterns emerging from the sample. By placing a lens tube, which acted as an iris, in front of the CCD camera, we matched the average speckle size to a single CCD pixel size. Ultrasonic bursts were synthesized by a function generator (Agilent, 33250A) and amplified by an RF amplifier (Amplifier Research, 75A250), and subsequently drove the ultrasound transducer. We used a low 1 Hz duty cycle to prevent damage to the transducer. The function generator triggered a pulse-delay generator (Stanford Research, DG535) that produced two CCD trigger pulses for each burst. The burst synchronized speckle pattern was captured with ultrasound; then, another one was captured without ultrasound. The exposure time of the CCD camera was equivalent to the duration of an ultrasonic burst. The laser speckle contrast was computed with and without ultrasound modulation. The UOT signal was defined as the change in speckle contrast between ultrasound on and off (off value – on value).

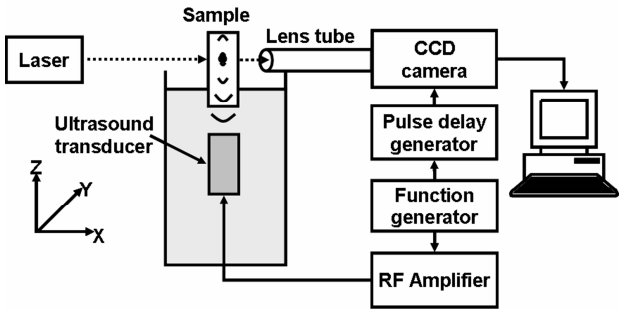


Figure 1: The UOT experimental Setup.

By irradiating the sample at two optical wavelengths, $\lambda_1$ and $\lambda_2$, independently, we obtained two UOT images that represent the distributions of light fluences at the two wavelengths. The dependence of the amplitude of the UOT signal on the local optical absorption was approximated to $\exp(-\mu_a d)$, where $\mu_a$ is the relative-local-optical absorption coefficient and $d$ is the diameter of an buried object. By using this dependence, we calculated the concentrations of both blue and red dyes. Therefore, the total dye concentration, $[R]+[B]$, and the ratio of the red dye concentration to the total dye concentration, $[R]/([R]+[B])$, can be calculated as follows:

$$[R]+[B]=\frac{\mu_a(\lambda_1)\Delta\varepsilon(\lambda_2)-\mu_a(\lambda_2)\Delta\varepsilon(\lambda_1)}{\varepsilon_B(\lambda_1)\varepsilon_R(\lambda_2)-\varepsilon_B(\lambda_2)\varepsilon_R(\lambda_1)}, \quad (1)$$

$$\frac{[R]}{[R]+[B]} = \frac{\mu_a(\lambda_2)\varepsilon_B(\lambda_1) - \mu_a(\lambda_1)\varepsilon_B(\lambda_2)}{\mu_a(\lambda_1)\Delta\varepsilon(\lambda_2) - \mu_a(\lambda_2)\Delta\varepsilon(\lambda_1)}, \quad (2)$$

where $[R]$ and $[B]$ are the concentrations of red and blue dyes, respectively, relative to their mother liquids; $\mu_a$ is the measured relative optical absorption; $\varepsilon_R$ and $\varepsilon_B$ are the relative absorption coefficients of pure red and blue mother liquids, respectively, measured with our UOT system; and $\Delta\varepsilon = \varepsilon_R - \varepsilon_B$.

## RESULTS AND DISCUSSIONS

The ratio of the ultrasound modulated light intensity to the unmodulated light intensity was computed using Monte Carlo simulations at different optical absorptions, and the simulated results were compared to the experimental results (Fig. 2). The Monte Carlo simulations are based on the temporal correlation transfer equation for acoustically modulated multiply scattered light.[10] This numerical method can map the distribution of ultrasound-modulated light intensity in isotropically optical scattering (scattering anisotropy: 0) medium containing heterogeneous optical properties and a nonuniform ultrasonic field.[10] The simulation parameters included a cylindrical-ultrasonic-focal zone of 2 mm in diameter and 20 mm in length, an ultrasonic pressure of 1.5 MPa, an optical wavelength of 633 nm, a 20 mm-thick isotropically scattering medium with a reduced scattering coefficient of ~9 $cm^{-1}$, and a cylindrical-optical-absorbing object of 2.2 mm in diameter and 11 mm in length. The optical absorption coefficient of the embedded object in the medium varied from 1 to 12 $cm^{-1}$. As the absorption coefficient increases, the UOT signal decreases as shown in Fig. 2. The decaying profile is close to an exponential fit instead of a linear fit. To validate our simulation results, we scanned a 20 mm-thick phantom containing five Trypan-Blue dyed objects (2.2 × 2.2 × 11 mm along the X, Y, and Z axes, respectively). The experimental parameters were the same as the above simulation parameters. Although they have different absolute values, the experimental and simulated results are highly correlated ($R^2$ value: 98%) as shown in Fig. 2.

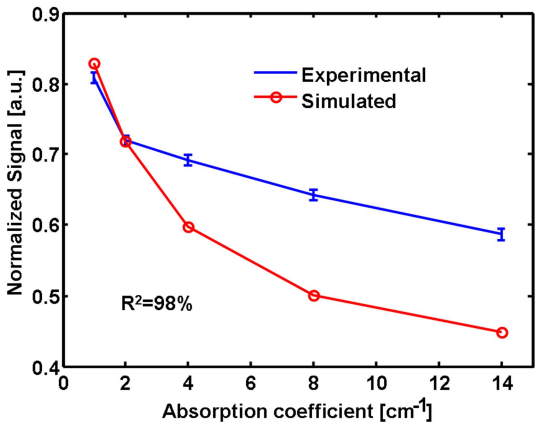


Figure 2: Comparison of simulated modulation depths and experimentally measured changes in speckle contrast at various values of optical absorption coefficient.

To investigate the potential of measuring HbT and $SO_2$ using UOT, we scanned a phantom at two optical wavelengths (633 nm and 657 nm). An acoustic peak pressure of 1 MPa was applied to the sample. The phantom was 20 mm thick and contained seven objects (Fig. 3a). The sizes of all seven targets were identical, 2.2 × 2.2 × 11 mm. Two dye solutions were mixed at six concentration ratios ($[R]$ : $[B]$ = 0:100, 30:70, 45:55, 75:25, 90:10, and 100:0 [%]) to mimic different levels of $SO_2$ (Fig. 3a.). Figure 3b shows 1D images obtained at the two optical wavelengths. By approximating the local amplitude of UOT signal (Fig. 3c.) to $\exp(-\mu_a d)$, we calculated each relative-local-optical absorption coefficient of six targets (Fig. 3d.). By substituting these relative optical absorption coefficients measured from the 1D images into Eqs. 1 and 2, we estimated the values of $[R]+[B]$ (Fig. 3e.) and $[R]/([R]+[B])$ (Fig.

3f.). The experimentally estimated total concentration $[R]+[B]$ in each of the six objects is close to the preset value of 100% with an error up to ~30%. The estimated $[R]/([R]+[B])$ values match well with the actual preset concentrations with an $R^2$ value of 99%.

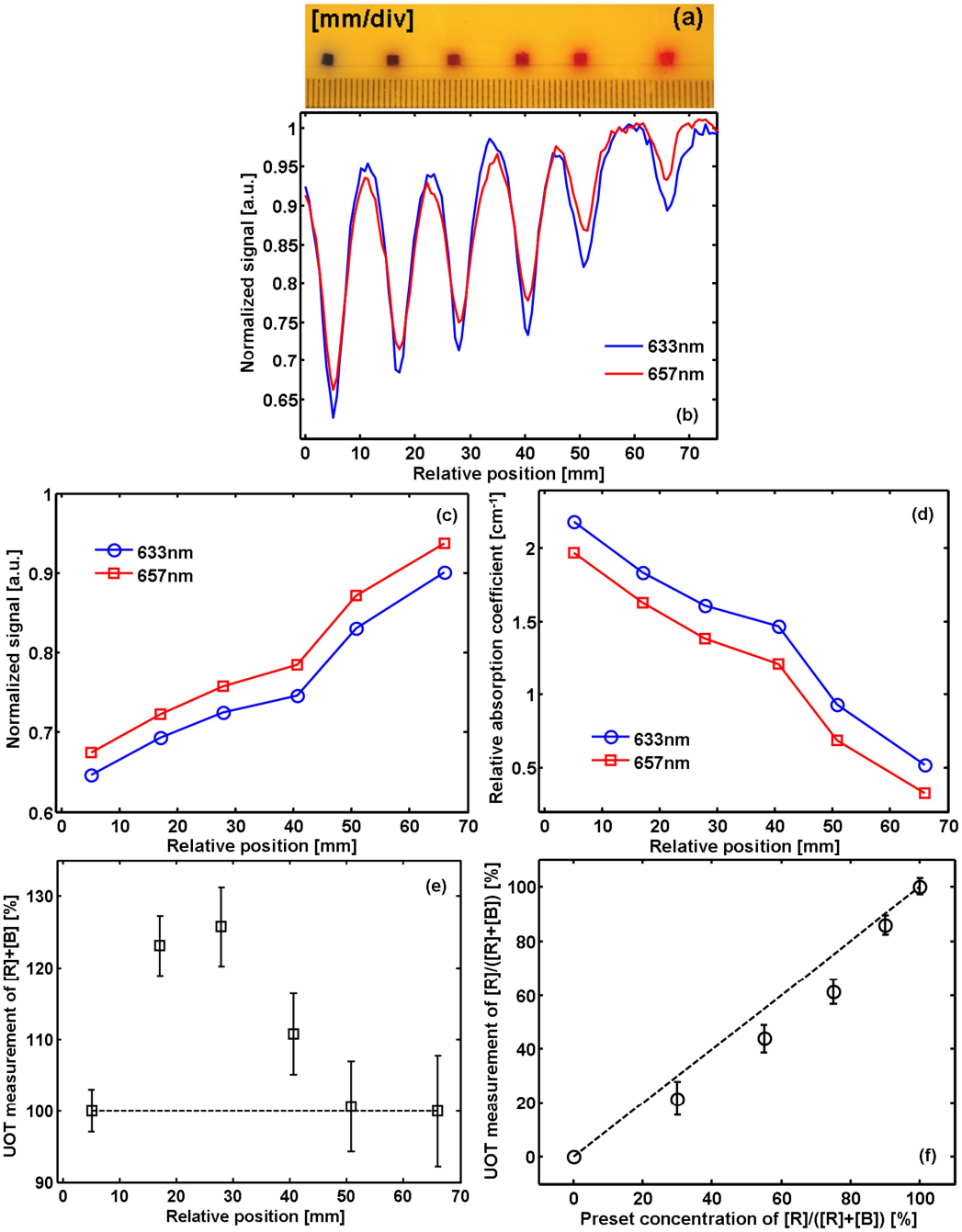


Figure 3: (a) Photograph of the tissue mimicking phantom containing six objects dyed with different ratios of red dye concentration, $[R]$, to the total dye (red and blue inks) concentration, $[R]+[B]$. (b) 1D images of the phantom at wavelengths of 633 nm and 657 nm. (c) Normalized change in speckle contrast at the position of each object, and (d) relative-local-optical absorption coefficient

of each object. (e) UOT measurements of the total dye concentration, $[R]+[B]$, and (f) the fraction of the red dye concentration in the total dye concentration, $[R]/([R]+[B])$.

## CONCLUSIONS

In conclusion, this research has demonstrated the feasibility of functional ultrasound-modulated optical tomography in tissue phantoms. The estimated total dye concentration and the ratio of the red dye concentration to the total dye concentration match the actual preset values well. The technique can potentially be extended to monitoring the total hemoglobin concentration and measuring the absolute hemoglobin oxygen saturation in vivo.

## ACKNOWLEDGEMENT

We thank Hao F. Zhang and Roger J. Zemp for fruitful scientific discussions. This research was supported by NIH Grant Nos. R33 CA 094267 and R01 CA106728.

## REFERENCES

[1] I. Vanzetta and A. Grinvald, "Increased cortical oxidative metabolism due to sensory stimulation: implications for functional brain imaging," Science. 286, 1555-1558 (1999).
[2] C. Chandrakala and D. L. Fraker, "Tumor oxygenation status as a prognostic marker," Can. Lett. 221, 225-235 (2005).
[3] J. P. Culver, A. M. Siegel, J. J. Stott, and D. A. Boas, "Volumetric diffuse optical tomography of brain activity" Opt. Lett. 28, 2016-2063 (2003).
[4] X. Wang, Y. Pang, G. Ku, X. Xie, G. Stoica, and L. V. Wang, "Noninvasive laser-induced photoacoustic tomography for structural and functional *in vivo* imaging of the brain," Nat. Biotech. 21, 803-806 (2003).
[5] H. F. Zhang, K. Maslov, G. Stoica, and L. V. Wang, "Functional photoacoustic microscopy for high-resolution and noninvasive *in vivo* imaging," Nat. Biotech. 24, 848–851 (2006).
[6] L. V. Wang, S. L. Jacques, and X. Zhao, "Continuous-wave ultrasonic modulation of scattered laser light to image objects in turbid media," Opt. Lett. 20, pp. 629–631 (1995).
[7] W. Leutz and G. Maret, "Ultrasonic modulation of multiply scattered light," Phys. B 204, pp. 14–19 (1995).
[8] L. V. Wang, "Mechanisms of ultrasonic modulation of multiply scattered coherent light: an analytic model," Phys. Rev. Lett. 87, (043093) pp. 1–4 (2001).
[9] S. Sakadzic and L. Wang, "Correlation transfer and diffusion of ultrasound-modulated multiply scattered light," Phys. Rev. Lett. 96, 163902 pp. 1–4 (2006)
[10] S. Sakadzic and L. V. Wang, "Correlation transfer equation for ultrasound-modulated multiply scattered light," Phys. Rev. E. 74, pp. 036618 1-10 (2006).
[11] S. Leveque, A. C. Boccara, M. Lebec, and H. Saint-Jalmes, "Ultrasonic tagging of photon paths in scattering media: parallel speckle modulation processing," Opt. Lett. 24, pp. 181–183 (1999).
[12] S. Sakadžic´ and L. V. Wang, "High-resolution ultrasound-modulated optical tomography in biological tissues," Opt. Lett. 29, pp. 2770-2772 (2004).
[13] T. W. Murray, L. Sui, G. Maguluri, R. A. Roy, A. Nieva, F. Blonigen, C. A. DiMarzio, "Detection of ultrasound-modulated photons in diffuse media using the photorefractive effect," Opt. Lett. 29, pp. 2509-2511 (2004).
[14] C. Kim, R. J. Zemp, and L. V. Wang, "Intense acoustic bursts as a signal-enhancement mechanism in ultrasound-modulated optical tomography," Opt. Lett. 31, pp. 2423–2425 (2006).
[15] R. J. Zemp, S. Sakadzˇic´, and L. V. Wang, "Stochastic explanation of speckle contrast detection in ultrasound-modulated optical tomography," Phys. Rev. E. 73, pp. 061920 1-5 (2006).
[16] X. Xu, H. Zhang, D. Qing, C. Kim, P. Hemmer, L. V. Wang, "Photorefractive detection of tissue optical and mechanical properties by ultrasound modulated optical tomography," Opt. Lett. 32, pp. 656–658 (2007).
[17] E. Bossy, A. R. Funke, K. Daoudi, and A. Boccara, "Transient optoelastography in optically diffusive media," Appl. Phys. Lett. 90, pp. 174111.1–174111.3 (2007).
[18] Diane Dalecki, "Mechanical bioeffects of ultrasound," Annu. Rev. Biomed. Eng. 6, pp. 18.1–18.20 (2004).
[19] A. Garcia-Uribe, N. Kehtarnavaz, G. Marquez, V. Prieto, M. Duvic, and L.V. Wang, "Skin cancer detection using spectroscopic oblique-incidence reflectometry: classification and physiological origins," App. Opt. 43 (13), pp. 2643–2650 (2004).